





Capability of Geomagnetic Storm Parameters to Identify Severe Space Weather

N. Balan^{1,2} , Qing-He Zhang¹, Zanyang Xing¹, R. Skoug³ , K. Shiokawa⁴, H. Lühr⁵, S. Tulasi Ram⁶, Y. Otsuka⁴, and Lingxin Zhao¹

¹Institute of Space Sciences, Shandong University, Weihai, Shandong 264209, People's Republic of China; balan.nanan@yahoo.com

²Institute of Geology and Geophysics, Chinese Academy of Sciences, Beijing 100029, People's Republic of China

³Los Alamos National Laboratory, Los Alamos, NM 87544, USA

⁴Institute for Space-Earth Environmental Research, Nagoya University, Nagoya 464-8601, Japan

⁵GFZ, German Research Centre for Geosciences, D-14473 Potsdam, Germany

⁶Indian Institute of Geomagnetism, Navi Mumbai, 410218, India

Received 2019 January 21; revised 2019 October 21; accepted 2019 October 22; published 2019 December 10

Abstract

The paper investigates the capability of geomagnetic storm parameters in the disturbance storm-time (Dst), Kp, and AE indices to distinguish between severe space weather (SvSW) that causes the reported electric power outages and/or telecommunication failures and normal space weather (NSW) that does not cause these severe effects in a 50 yr period (1958–2007). The parameters include the storm intensities DstMin (minimum Dst during the main phase, MP, of the storm), $(d\text{Dst}/dt)_{\text{MPmax}}$, K_{pmax} , and AE_{max} . In addition, the impulsive parameter $\text{IpsDst} = (-1/T_{\text{MP}}) \int_{T_{\text{MP}}} |\text{Dst}_{\text{MP}}| dt$ is derived for the storms that are automatically identified in the Kyoto Dst and USGS Dst. $\int_{T_{\text{MP}}} |\text{Dst}_{\text{MP}}| dt$ is the integral of the modulus of the Dst from onset of the MP (MPO) to the DstMin. T_{MP} is the MP duration from MPO to DstMin. The corresponding mean values $\langle K_{\text{pMP}} \rangle$ and $\langle \text{AE}_{\text{MP}} \rangle$ are also calculated. Regardless of the significant differences in the storm parameters between the two Dst indices, the IpsDst in both indices seems to identify four of the five SvSW events (and the Carrington event) in more than 750 NSW events that have been reported to have occurred in 1958–2007, while all other parameters separate one or two SvSWs from the NSWs. Using the Kyoto IpsDst threshold of -250 nT, we demonstrate a 100% true SvSW identification rate with only one false NSW. Using the false NSW event (1972 August 4), we investigate whether using a higher resolution Dst might result in a more accurate identification of SvSWs. The mechanism of the impulsive action leading to large IpsDst and SvSW involves the coincidence that the fast interplanetary coronal mass ejection velocity V contains its shock (or front) velocity ΔV and large interplanetary magnetic field B_z southward covering ΔV .

Unified Astronomy Thesaurus concepts: Space weather (2037); Geomagnetic fields (646); Solar wind (1534)

1. Introduction

A series of rapid changes takes place in interplanetary space and the environment of planets during the passage of interplanetary coronal mass ejections (ICMEs; e.g., Witasse et al. 2017), high-speed streams, and corotating interaction regions (Smith & Wolfe 1976). The changes are collectively called space weather. An ICME is a huge, magnetized (with an interplanetary magnetic field, IMF, up to 100 nT), high-density (up to 100 cm^{-3}) plasma cloud that is ejected from the Sun and flows out with speeds of up to thousands of km s^{-1} (e.g., Skoug et al. 2004). However, the part of the ICME that is most geoeffective is the magnetic cloud, which is a region with a high magnetic field but a low density (Burlage et al. 1981). A high-speed ICME produces shock waves ahead, which accelerate the background-charged particles to energies over 100 MeV, which are known as solar energetic particles (e.g., Singh et al. 2010). The particles are accelerated to even higher energies by the high-speed ICME front that follows the ICME shock (e.g., Balan et al. 2014). They can damage satellite systems (e.g., Green et al. 2017) and are harmful for biological systems, for example, astronauts (e.g., Aran et al. 2005).

In the Earth's environment, space weather includes sudden changes (or disturbances) in the magnetosphere, ring currents, radiation belts, geomagnetic fields, auroras, in the ionosphere, and in the thermosphere. The disturbances in the geomagnetic field that last from several hours to several days and are produced

by the intensification of magnetospheric current systems are called geomagnetic storms (Svalgaard 1977; Gonzalez et al. 1994; Lühr et al. 2017). The current systems contribute differently to the storms in different latitudes; and the storms are therefore identified by indices such as the low-latitude disturbance storm-time (Dst) index (Sugiura 1964; Love & Gannon 2009), the mid-latitude Kp index, and the high-latitude AE index (e.g., Rostoker et al. 1995). Another index that is sometimes used is the rate of change of the horizontal component (dH/dt) of the geomagnetic field. The Dst storms arise mainly from the intensification of the ring current due to ICME–magnetosphere coupling and ionosphere–ring current coupling, the efficiency of which has been studied using solar wind and IMF data and models (e.g., Burton et al. 1975; Fok et al. 2001; Newell et al. 2007; Liemohn et al. 2010). The storms become more intense with the increase in the solar wind velocity V and strength of IMF B_z southward (e.g., Ebihara et al. 2005). Based on the minimum value of the Dst (DstMin) that is reached during the main phase (MP) of the storm, the storms are classified into moderate storms ($-100 < \text{DstMin} \leq -50$ nT), intense storms ($-250 < \text{DstMin} \leq -100$ nT), and super storms ($\text{DstMin} \leq -250$ nT) (e.g., Gonzalez et al. 1994).

Scientific analysis of solar storms and geomagnetic storms leads to a fundamental understanding of the Earth's surrounding space weather (e.g., Gopalswamy et al. 2005; Kamide & Balan 2016). Application-oriented analysis of the storms enables the assessment and mitigation of space weather hazards

on satellite systems, satellite communication and navigation, electric power grids, telecommunication systems, etc. Of particular concern are the effects associated with extreme storms (e.g., Boteler 2001; Pulkkinen 2007; Viljanen et al. 2010; Hapgood 2011; Love et al. 2017). If a space weather event similar to the Carrington event of 1859 September 1–2 (Carrington 1859) were to occur today, it might cause very serious impacts in our high-tech society (e.g., Baker et al. 2008; Schrijver et al. 2015; Eastwood et al. 2017). It is therefore important for both scientific and technological reasons to identify some parameters of the storms that can indicate their severity.

Conventionally, the DstMin, the maximum rate of change of the Dst during the MP ($d\text{Dst}/dt$)_{MPmax}, and maximum values of the Kp and AE (Kp_{max} and AE_{max}), all representing geomagnetic storm intensities, have been used for investigating the space weather in Earth’s environment. However, while studying what determines the severity of the space weather (Balan et al. 2014), we realized that the DstMin is an insufficient indicator of severe space weather (SvSW), as reported also by Cid et al. (2014). We define SvSW as causing the reported electric power outages and/or telecommunication failures and normal space weather (NSW) as not causing such severe effects in a 50 yr period (1958–2007). Our studies also showed that the mean value of the Dst during the MP ($\langle\text{Dst}_{\text{MP}}\rangle$) can indicate the severity of space weather (Balan et al. 2016). The $\langle\text{Dst}_{\text{MP}}\rangle$ can also be used as a better reference than the DstMin in developing a scheme for forecasting SvSW using ICME velocity and magnetic field (Balan et al. 2017a). The derived parameter ($\langle\text{Dst}_{\text{MP}}\rangle$) is hereafter be called *IpsDst* (Section 2).

In a brief report (Balan et al. 2016), we introduced *IpsDst*, indicating the impulsive (*Ips*) strength of Dst storms to distinguish between SvSW and NSW using only the super storms (DstMin ≤ -250 nT) in the Kyoto Dst data. No other data were used. The present paper investigates the capability of the important storm parameters in the Dst, Kp, and AE indices to distinguish between the SvSW and NSW events that have been reported to have occurred in a 50 yr period (1958–2007). In addition to the conventional parameters mentioned above, the paper uses the *IpsDst* for the Dst storms that are automatically identified in the widely used Kyoto Dst and new (and improved) USGS Dst data in 1958–2007. The paper also uses the mean values of the Kp and AE during the MP ($\langle\text{Kp}_{\text{MP}}\rangle$ and $\langle\text{AE}_{\text{MP}}\rangle$) in the same 50 yr period. The SvSW events include the event on 1972 August 4, which was missed in Balan et al. (2016) because it occurred during a non-super storm (DstMin -125 nT). It has puzzled the scientific community because all other SvSW events (including the Carrington event of 1859 September 1–2) occurred during super storms. The paper also explains the physical significance of the *IpsDst* and discusses the physical mechanism leading to large *IpsDst* and SvSW using the solar wind and IMF data from the *Advanced Composition Explorer* (ACE) satellite that have been available since 1998.

Section 2 describes the data and analysis. The results are presented and discussed in Sections 3 and 4. The SvSW events that have been reported to have occurred in the 50 yr period (1958–2007) and the Carrington SvSW event only are investigated. The SvSW events reported occurring prior to the Dst era (Davidson 1940; Cliver & Dietrich 2013; Love & Coïsson 2016; Ribeiro et al. 2016; Love 2018) are discussed in

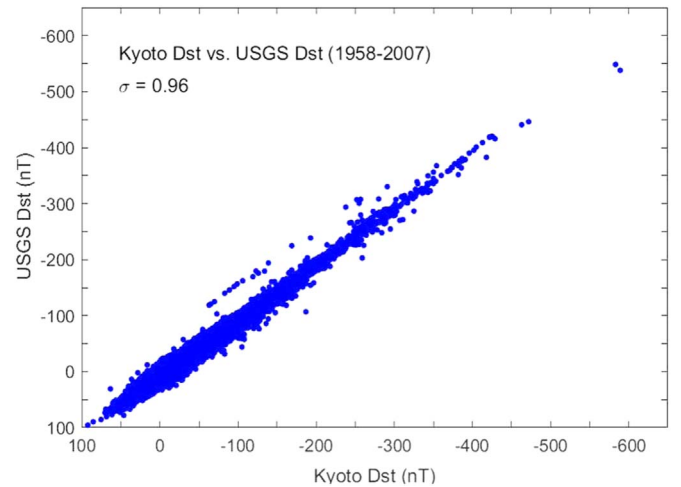


Figure 1. Scatter plot of hourly Kyoto Dst against USGS Dst in 1958–2007.

Section 4, but they are not investigated for the lack of Dst data. Minor technological problems such as capacitor stripping in power transformers (e.g., Kappenman 2003) will be included later using high-resolution *IpsDst*.

2. Data and Analysis

The hourly Kyoto Dst and USGS Dst data covering a 50 yr time period (1958–2007) are available at <http://wdc.kugi.kyoto-u.ac.jp/dstdir/> and <http://geomag.usgs.gov/data>, respectively. The primary difference between the Kyoto Dst (Sugiura 1964; Sugiura & Kamei 1991) and USGS Dst (Love & Gannon 2009) is in the removal of secular and solar quiet (Sq) variations. The Kyoto Dst partially removes these variations and USGS Dst more fully removes them, which results in an offset between the two indices. Love & Gannon (2009) presented a panoramic view of the two indices for the whole 50 yr period and detailed comparisons for selected 40-day time segments. They reported a significant offset (Kyoto minus USGS) of up to -70 nT between the indices. Figure 1 shows a scatter plot of the indices in the 50 yr period. The indices have a correlation of 0.96 and the offset is mainly negative. The average offset is -8.50 nT in all data together and -5.0 nT in quiet-time (Dst > -25 nT) data alone (Balan et al. 2017b). For the Carrington storm, the H-component data measured at Bombay (Tsurutani et al. 2003) and calculated by Cliver & Dietrich (2013) are used. The Kp and AE data are available at <http://wdc.kugi.kyoto-u.ac.jp/kp/index.html> and <http://wdc.kugi.kyoto-u.ac.jp/aedir/>, respectively.

The Dst storms were automatically identified by a computer program that uses four selection criteria. The criteria are (1) DstMin ≤ -50 nT and $T_{\text{MP}} > 2$ hr, (2) absolute value of the MP range, that is, $|\text{Dst}_{\text{MPO}} - \text{DstMin}| \geq 50$ nT, (3) separation between DstMin and next MPO ≥ 10 hr, and (4) rate of change of Dst during the MP or $(d\text{Dst}/dt)_{\text{MP}} < -5$ nT hr⁻¹. MPO here stands for MP onset. The selection criteria minimize non-storm-like fluctuations (Balan et al. 2017b). The computer program identified 761 storms in the Kyoto Dst, which include 34 super storms, 296 intense storms, and 431 moderate storms. The 585 storms identified in USGS Dst include 33 super storms, 210 intense storms, and 342 moderate storms. Figure 2 compares four super storms in the two indices. Intense and moderate storms were compared before (Balan et al. 2017b). Although the storms in the two indices exhibit similar

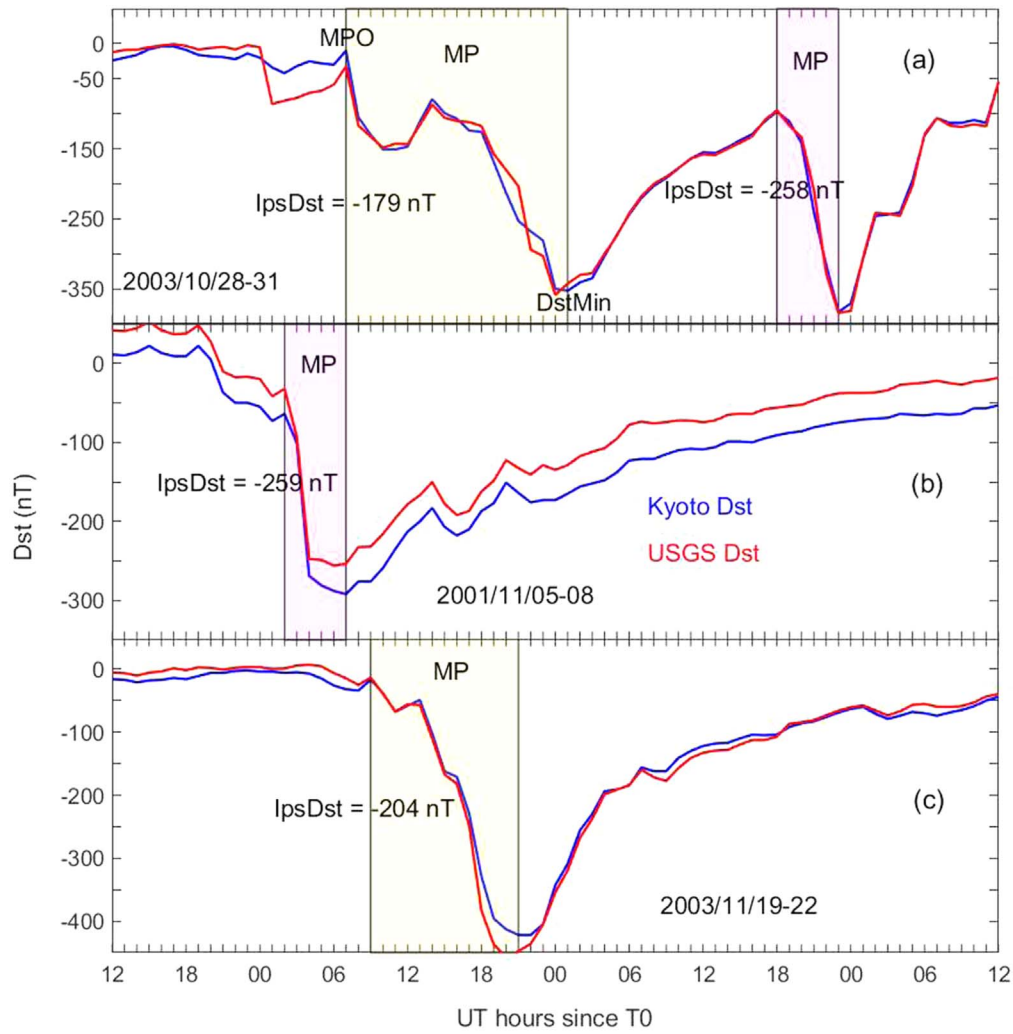


Figure 2. Comparison of four super storms ($Dst_{Min} \leq -250$ nT) in the Kyoto Dst (blue) and USGS Dst (red) having large IpsDst (purple shade) and comparatively weak IpsDst (yellow shade). MPOs are identified by a computer program satisfying storm selection criteria and IMF Bz turning southward. The time T0 of the X-axis corresponds to 12 UT on 2003 October 28 (a), 2001 November 5 (b), and 2003 November 19 (c).

variations, they have differences in the DstMin and in its time of occurrence, which can cause differences in the IpsDst.

2.1. Parameter IpsDst

The parameter *IpsDst* is defined as $IpsDst = (-1/T_{MP}) \int_{T_{MP}} |Dst_{MP}| dt$ (Balan et al. 2014). $\int_{T_{MP}} |Dst_{MP}| dt$ is the integral (or sum) of the modulus of the Dst from MPO to DstMin. MPO is the MP onset time when the Dst starts to decrease, satisfying the storm selection criteria (and IMF Bz turning southward), which is also the peak of the sudden storm commencement (SSC). T_{MP} is the time interval (or duration) from MPO to DstMin. The rate of change of the Dst during the MP and its maximum value $(dDst/dt)_{MPmax}$ are obtained. By definition, the IpsDst includes most important characteristics of Dst storms (SSC, MPO, $(dDst/dt)_{MPmax}$, DstMin, and T_{MP}) and gives the mean value of the Dst during the MP when most energy input occurs (Figure 2). IpsDst is proportional to the total amount of energy input during MP (e.g., Burton et al. 1975) divided by the duration of energy input. The higher the energy input and the shorter the duration, the higher the IpsDst value and the more impulsive its action, and so the name IpsDst. The

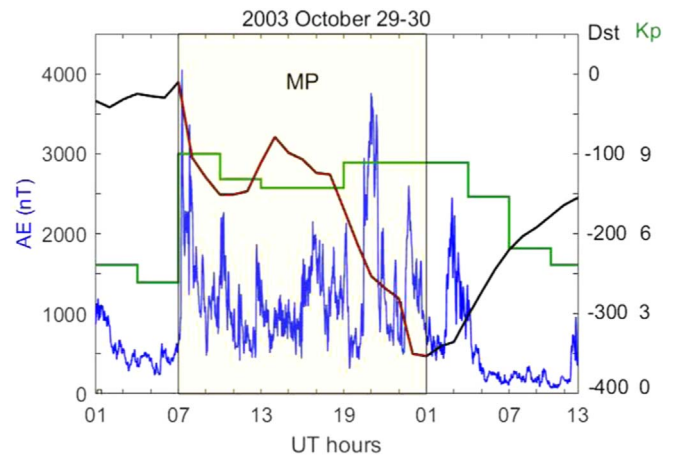


Figure 3. An example identifying the storm MP in the Dst, Kp, and AE storms.

maximum values of the Kp and AE storms (Kp_{max} and AE_{max}) are noted. Their MP durations corresponding to the MP of Dst storms are identified, as shown with an example in Figure 3. The mean values of Kp and AE during the storm MP are

Table 1
Number, Dates, and Parameter Values in the Order of IpsDst in Figure 6

No. and Date	−IpsDst (nT)	T_{MP} (hr)	−DstMin (nT)	$(dDst/dt)_{MPmax}$ (nT/hr)	F10.7	SvSW/NSW
1. 1859 Sep 1	700 ± 100	2	1710	1390	nan	SvSW
2. 1989 Mar 13	357 ± 22	16	589	111	253	SvSW
3. 1958 Feb 11	275 ± 34	8	426	103	224	SvSW
4. 2001 Nov 6	259 ± 52	5	292	168	233	SvSW
5. 2003 Oct 30	258 ± 52	5	383	98	268	SvSW
6. 2001 Mar 31	238 ± 48	5	387	148	245	NSW
7. 1981 Apr 13	235 ± 34	7	311	75	255	NSW
8. 1967 May 26	230 ± 19	12	387	106	219	NSW
9. 2004 Nov 10	229 ± 25	9	263	43	103	NSW
10. 1989 Oct 21	220 ± 20	11	268	61	206	NSW
11. 1960 Apr 1	217 ± 24	9	327	56	201	NSW
12. 2004 Nov 8	209 ± 19	11	374	96	122	NSW
13. 2003 Nov 20	204 ± 17	12	422	100	171	NSW
14. 1959 Jul 15	204 ± 19	11	429	92	253	NSW
15. 1958 Sep 4	201 ± 22	9	302	55	261	NSW
16. 1991 Oct 29	188 ± 24	8	254	29	269	NSW
17. 1991 Nov 9	187 ± 16	12	354	61	194	NSW
18. 1960 Apr 30	184 ± 31	6	325	151	164	NSW
19. 2000 Apr 6	183 ± 23	8	288	74	178	NSW
20. 2003 Oct 29	179 ± 10	18	353	95	275	NSW
21. 1989 Nov 17	179 ± 14	13	266	52	215	NSW
22. 1982 Sep 6	174 ± 15	12	289	44	172	NSW
23. 2000 Jul 15	172 ± 19	9	301	137	220	NSW
24. 1958 Jul 8	170 ± 13	13	330	92	240	NSW
25. 1982 Jul 14	163 ± 18	9	325	110	269	NSW
26. 1991 Mar 25	157 ± 16	10	298	63	235	NSW
27. 1970 Mar 8	156 ± 20	8	284	90	173	NSW
28. 1961 Oct 28	154 ± 17	9	272	62	86	NSW
29. 2001 Apr 11	145 ± 18	8	271	58	160	NSW
30. 1960 Nov 13	142 ± 8	17	339	81	178	NSW
31. 1990 Apr 10	133 ± 7	20	281	45	149	NSW
32. 1960 Oct 7	120 ± 4	28	287	45	145	NSW
33. 1972 Aug 4	112 ± 22	5	125	35	125	SvSW
34. 1992 May 10	111 ± 6	18	288	62	127	NSW
35. 1989 Sep 19	106 ± 8	14	255	40	197	NSW
36. 1986 Feb 8	105 ± 2	47	307	71	94	NSW

Note. Table lists the storm numbers and dates of IpsDst in Figure 6(a) and the corresponding other parameters, including SvSW/NSW. The values of the other parameters in Figure 6 do not correspond to the same number and date because of their increasing or decreasing ordering.

calculated as

$$\langle Kp_{MP} \rangle = \Sigma Kp_{MP} / T_{MP} \text{ and } \langle AE_{MP} \rangle = \Sigma AE_{MP} / T_{MP}.$$

$\langle Kp_{MP} \rangle$ and $\langle AE_{MP} \rangle$ might represent the impulsive strength of the Kp and AE storms because they give the mean values of Kp and AE during the storm MP when most energy input occurs.

The accuracy of IpsDst depends on the accuracy of the Dst data and T_{MP} . According to Sugiura (1964), who developed the Dst index, it is not easy to compute the uncertainty of the Dst (T. Iyemori 2019, private communication). The uncertainty includes the measurement errors at the four Dst observatories, errors associated with the selection of five quiet days for each month, and errors due to the variation of the quiet-time ring current when the Dst is zero. These errors are mostly removed in the final version of the Dst, especially in USGS Dst (Love & Gannon 2009). The uncertainty also seems to depend on the time when a storm actually hits the Dst stations and the time when the Dst shows the storm. However, this difference in time may not cause a significant difference in the Dst because the ring current starts to develop not at a specific point in time, but during a certain range in time (M. Nose 2019, private communication). The accuracy of T_{MP} depends on the accurate

identification of the times of MPO and DstMin. The computer program identifies these times following the selection criteria. The MPO times of the storms since 1998, when ACE data are available, are also found to agree with the times of IMF Bz turning southward. The time resolution (1 hr) of the Dst data, however, can cause significant uncertainty in IpsDst. It causes ± 30 minutes uncertainty in the identification of MPO and DstMin or an uncertainty ΔT_{MP} of ± 1 hr in T_{MP} . The corresponding uncertainty in IpsDst is $\Delta IpsDst = \pm IpsDstx(\Delta T_{MP}/T_{MP})$. Table 1 lists the computed IpsDst and its uncertainty of all 35 super storms and the intense storm on 1972 August 4. It assumes that the uncertainty in the Dst is negligible compared to that in T_{MP} . The uncertainty in general decreases with increasing (negative) IpsDst.

The offset between the two Dst indices causes differences in their storm parameters. Figure 4 shows the absolute and percentage differences (Kyoto minus USGS) in DstMin and IpsDst of the storms as a function of time, with red for super storms and blue for intense and moderate storms together. Although the absolute difference is mainly negative up to -54 nT in DstMin (Figure 4(a)) and -58 nT in IpsDst (Figure 4(c)), it is also positive up to 20 nT in DstMin and 84 nT in IpsDst for

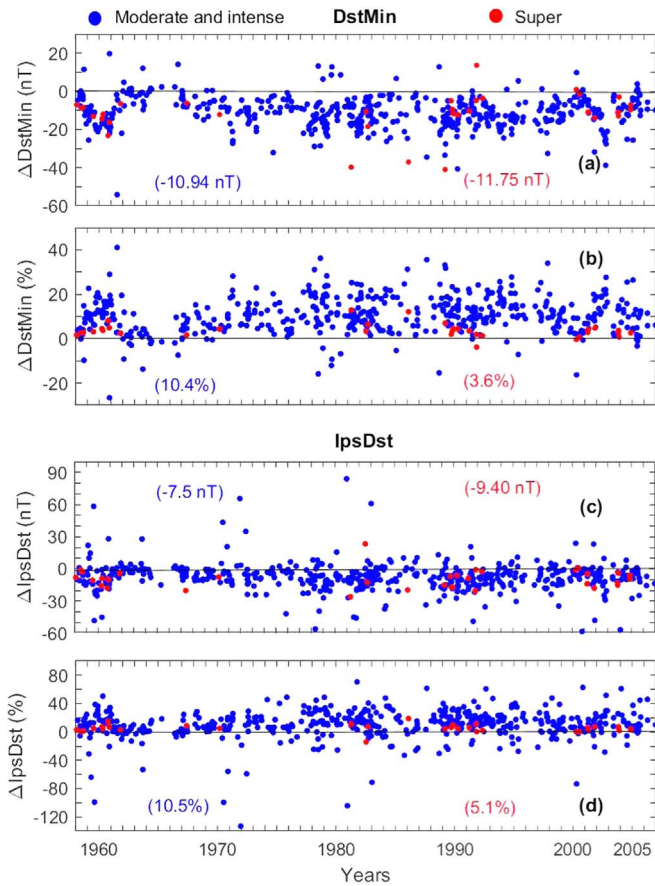


Figure 4. Scatter plot of the absolute and percentage differences (Kyoto minus USGS) in DstMin (a), (b) and IpsDst (c), (d) of the storms in the two Dst indices as a function of time, with red for super storms and blue for intense and moderate storms together. The average differences are noted in the parentheses.

a small number of storms. The percentage difference is positive up to 40% in DstMin (Figure 4(b)) and 65% in IpsDst (Figure 4(d)), although it is negative up to -35% in DstMin and -130% in IpsDst for a small number of storms. The average differences noted in the figure are smaller in IpsDst than in DstMin by about 2 nT on the whole, although their percentage differences are nearly equal. T_{MP} (not shown) is found equal for about half of the storms and differs for the others, resulting in an average difference of -0.28 hr overall. T_{MP} differs generally because the DstMin in one index occurs slightly later or earlier than in the other index (Figure 2). As discussed, there are significant offsets between the two Dst indices and differences in their storm parameters. It therefore becomes interesting to investigate how well the various important storm parameters in the two Dst indices and in the Kp and AE indices work in distinguishing between the SvSW and NSW events.

The ACE satellite at the L1 point has provided IMF and solar wind data continuously since 1998. The velocity and density data in the Solar Wind Ion (SWI) mode of the Solar Wind Electron Proton Alpha Monitor instrument at 64 s resolution (e.g., McComas et al. 1998; Skoug et al. 2004) are available at Caltech (<http://www.srl.caltech.edu/ACE/ASC/>). During high-energy particle events, when the SWI mode may not cover the full solar wind flux distribution, the 64 s data collected in the Search/Supra Thermal Ion mode once every ~ 32 minutes are used. The data (time) are corrected for the ACE–Earth distance. The velocity

and IMF data for the Carrington, Quebec, 1958 February, and 1972 August events are adopted from the calculations by Cliver & Svalgaard (2004), Nagatsuma et al. (2015), Cliver et al. (1990), and Vaisberg & Zastenker (1976), respectively.

To discuss the mechanism that connects the Dst storms and solar storms (Section 4.3), we define the beginning of an ICME event as the time when the solar wind velocity (V) suddenly increases to high values (Balan et al. 2014). The ICME event front (or shock) velocity ΔV is the difference between the peak ICME velocity and the upstream slow solar wind velocity (V). The velocity, especially during severe events measured with 32-minute resolution, is found to take about two hours to reach its peak. ΔV in general is therefore taken as the difference between the mean velocity for 2 hr after and 2 hr before the start of the velocity increase. B_z at ΔV ($B_{z\Delta V}$) is the mean of B_z for the two hours from the start of the velocity increase.

3. Identification of SvSW

3.1. Definition and Events

As mentioned in Section 1, the space weather events that have been reported to have caused electric power outages and/or telegraph system failures in the 50 yr period (1958–2007) are defined as SvSW. Five such SvSW events are reported to have occurred in 1958–2007. The event of 1958 February 11 damaged telegraph systems in Sweden (e.g., Wik et al. 2009) and caused electric power supply problems in the US (Slothower & Albertson 1967). The event of 1972 August 4 caused telecommunication failure and electric power supply problems in the US (Albertson & Thorson 1974; Anderson et al. 1974). The Quebec event of 1989 March 13 (e.g., Medford et al. 1989) and the New Zealand event of 2001 November 6 (Marshall et al. 2012) caused electric power outages. The Halloween event of 2003 October 30 caused an electric power outage in Sweden (e.g., Pulkkinen et al. 2005). The Carrington event of 1859 September 1–2 that caused telegraph system failures (Loomis 1861) is also included. All other space weather events that occurred in the 50 yr period are considered NSW events because they are not reported to have caused such severe effects.

3.2. Identification

Using the DstMin and IpsDst, we attempt to determine their abilities to differentiate between SvSW and NSW events for each of the two Dst indices. Figure 5 shows scatter plots of the IpsDst against DstMin considering all common storms in 1958–2007. For the Carrington storm (right-hand top event), the equivalent DstMin and IpsDst are limited to -650 nT and -450 nT, respectively. Red and green represent SvSW in the Kyoto Dst and USGS Dst, respectively. The regions marked 1–2 and 2–3 represent the IpsDst ranges of NSW and SvSW events, including the uncertainty in IpsDst due to the uncertainty in T_{MP} of the respective highest and lowest IpsDst values. IpsDst seems able to mostly differentiate between the populations of SvSW and NSW in both Dst indices. Using DstMin only allows for the separation of two out of the six events. Due to the single SvSW event (1972 August 4) that is not separated by the IpsDst, there appears a very wide range of IpsDst that can cause SvSW and the distribution overlaps with that of NSW. We discuss the 1972 August 4 SvSW event in Section 4.1.

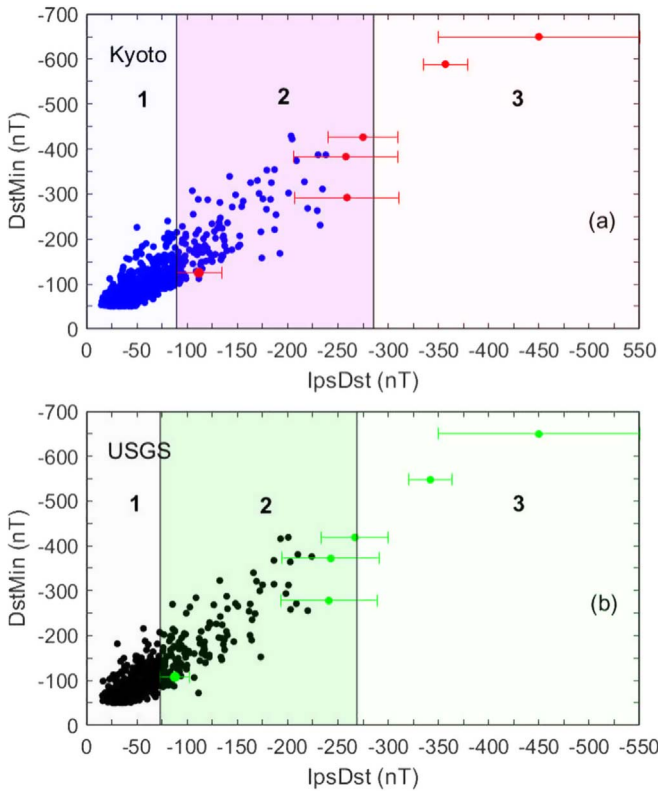


Figure 5. Scatter plot of the IpsDst against DstMin of the Carrington storm and all common storms during 1958–2007 in (a) the Kyoto Dst and (b) USGS Dst. Red and green dots correspond to SvSW events. Regions 1–2 and 2–3 represent the IpsDst ranges of NSW and SvSW events, including the uncertainty in IpsDst due to the uncertainty in T_{MP} of the highest and lowest IpsDst values, respectively. The horizontal bars show the uncertainty in IpsDst of the SvSW events only for simplicity and limited to ± 100 nT for the Carrington event.

Next, we include other important storm parameters. Although we analyzed all storms, the parameters are shown only for all super storms, the intense storm of 1972 August 4, and the Carrington storm. Figure 6 displays the IpsDst, T_{MP} , DstMin, and $(dDst/dt)_{MPmax}$ in the Kyoto Dst; the solar activity index F10.7 on the days of DstMin is also shown. For the Carrington event (number 1), the equivalent DstMin, IpsDst, and $(dDst/dt)_{MPmax}$ are limited to -650 nT, -450 nT, and 200 nT/hr, respectively, for better display with the other parameters in the figure. All parameters are arranged in their respective increasing or decreasing orders. Red and blue represent SvSW and NSW events, respectively. Table 1 lists the IpsDst together with its uncertainty and other parameters for each of the storms shown in Figure 6. The IpsDst best separates SvSW from NSW, although the outlier of event number 33 (1972 August 4) has a significantly weak IpsDst (-112 nT), which we discuss in Section 4.1.

Figure 7 is similar to Figure 6, but for USGS Dst with green and black representing SvSW and NSW events, respectively. The offset between the two Dst indices results in the absence of one super storm in USGS Dst. The differences in the respective storm parameter values between the two indices result in some differences in the order number of the parameters in Figure 7 compared to Figure 6. For these reasons, F10.7 is also shown in Figure 7. The behavior of all parameters in USGS Dst is similar to that in the Kyoto Dst.

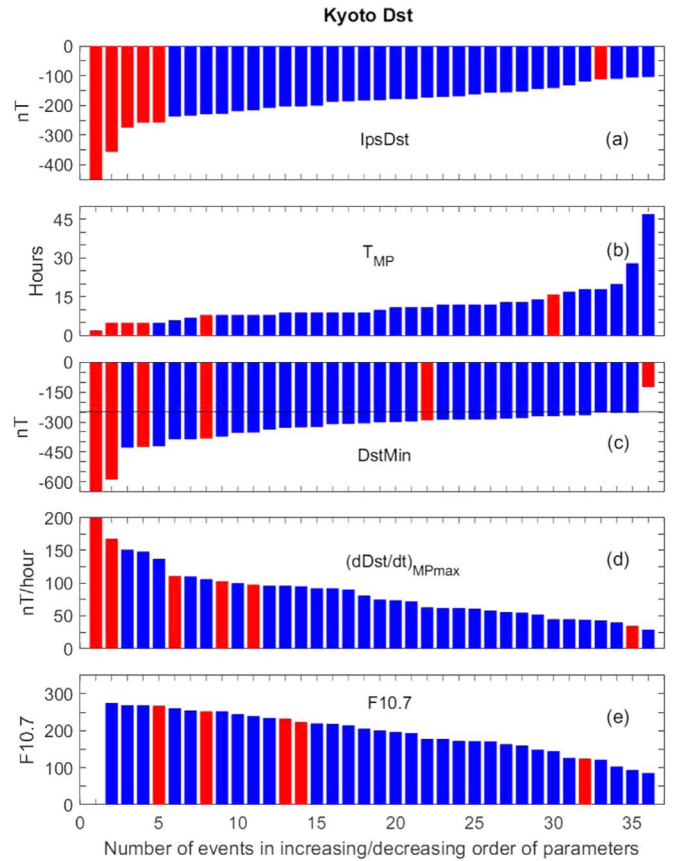


Figure 6. IpsDst, T_{MP} , DstMin, $(dDst/dt)_{MPmax}$, and F10.7 on the days of DstMin of the super storms ($DstMin \leq -250$ nT) in the Kyoto Dst arranged in their increasing or decreasing orders. The Carrington storm of 1859 and the intense storm on 1972 August 4 are included. Red corresponds to SvSW and blue to NSW (see text).

3.3. Kp and AE Indices

Because SvSW effects usually occur at high latitudes, one might expect the high- and mid-latitude indices (AE and Kp) could also be used to distinguish between SvSW and NSW events. However, these indices are inadequate, as illustrated in Figure 8, which shows $\langle Kp_{MP} \rangle$, Kp_{max} , $\langle AE_{MP} \rangle$, and AE_{max} corresponding to the Dst storms in Figure 6(a). The parameters are arranged in their respective decreasing orders. Red and blue correspond to SvSW and NSW, respectively. In Figure 8(a), the SvSW events from left to right correspond to the storms in 2001 November, 2003 October, 1958 February, 1989 March, and 1972 August. The Carrington event has no Kp data, and five events, including the Carrington and 1972 August 4 events, have no AE data. In all parameters (Figure 8), the SvSW events are mixed with NSW events. AE and Kp seem inadequate to distinguish between SvSW and NSW mainly because they do not distinguish their phases when a majority of energy input occurs. The Kp is also a 3 hr index, and AE can sometimes reach maximum before the main energy input starts from the MPO of Dst storms.

4. Discussion

As mentioned in Section 1, Dst storms have been studied and modeled for many years using the Dst index, solar wind, and IMF data. The models have improved our understanding of the mechanisms connecting Dst storms and solar storms. For

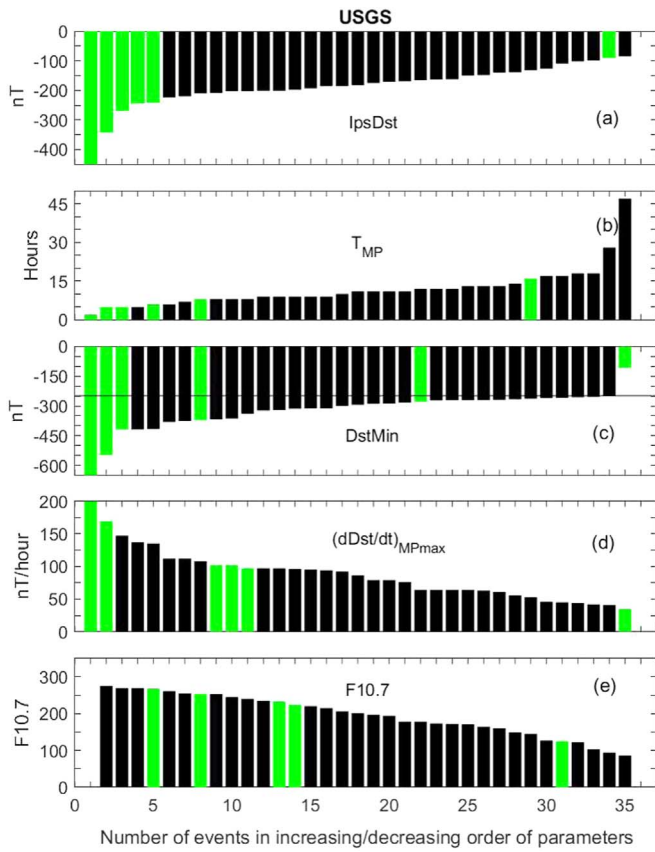


Figure 7. IpsDst, T_{MP} , DstMin, $(dDst/dt)_{MPmax}$, and F10.7 on the days of DstMin of the super storms (DstMin ≤ -250 nT) in USGS Dst arranged in increasing or decreasing orders of the parameters. The Carrington storm of 1859 and intense storm on 1972 August 4 are included. Green corresponds to SvSW and black to NSW (see text).

example, using V , N (density), and Bz , Burton et al. (1975) modeled the seven Dst storms in 1967–1968. Klimas et al. (1997) presented a method for transforming a linear prediction model into linear and nonlinear dynamical analogs of the coupling between the input and output data. Using VBz for input and Dst for output, they showed that the nonlinear analog couples to the solar wind through the expression $(VBz/Dst) \times VBz$ rather than through the usual linear dependence on VBz. The multi-input (VBz and dynamic pressure P) and single-output (Dst) discrete-time model developed by Zhu et al. (2007) explains the Dst dynamics more accurately than previous models. Using USGS Dst and a lognormal stochastic process, Love et al. (2015) reported that the most extreme Dst storms (DstMin ≤ -850 nT) can occur ~ 1.13 times per century, with 95% confidence level. The ICME-magnetosphere coupling function developed by Newell et al. (2007) is a good measure of the coupling efficiency, although it is still not able to distinguish between SvSW and NSW (Balan et al. 2017a).

By definition, the parameter IpsDst = $(-1/T_{MP}) \int_{T_{MP}} |Dst_{MP}| dt$ gives the mean value of the Dst during the storm MP (Figure 2), and therefore indicates the impulsive strength of Dst storms (IpsDst). The important result from Section 3 is that regardless of the significant offset and differences between the two Dst indices, the impulsive parameter IpsDst in both indices seems more likely to distinguish between SvSW and NSW events than other common Dst-based parameters. Using a truth table, we calculate the success of the identification. Table 2 lists the number of (a) true SvSW,

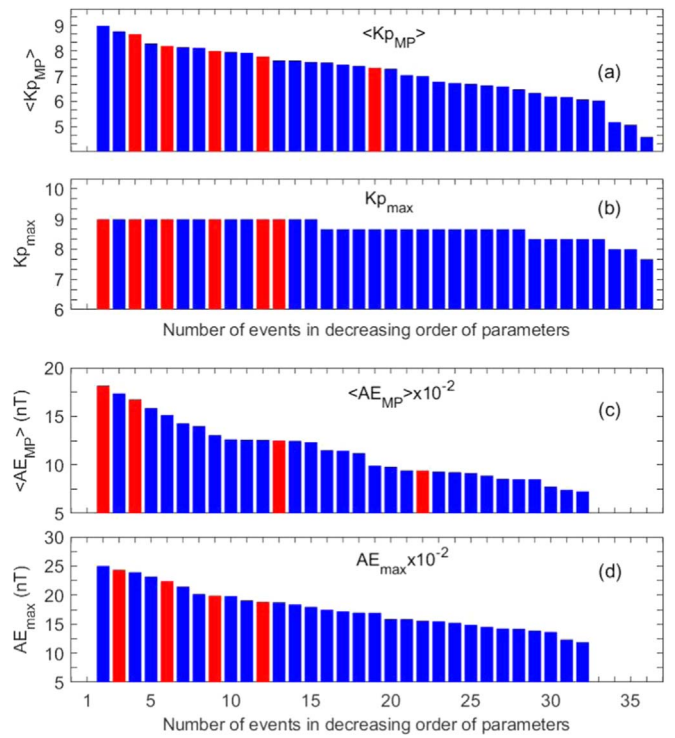


Figure 8. $\langle Kp_{MP} \rangle$, Kp_{max} , $\langle AE_{MP} \rangle \times 10^{-2}$, and $AE_{max} \times 10^{-2}$ arranged in their decreasing orders. The parameters correspond to the Dst storms shown in Figure 6(a). The Carrington event has no Kp data, and five events, including the Carrington and 1972 August 4 events, have no AE data. Red and blue correspond to SvSW and NSW, respectively.

Table 2
Truth Table

Total = 762	Identified	
	True	False
Actual SvSW	$a = 5$	$b = 0$
Actual NSW	$c = 756$	$d = 1$

Note. The truth table lists the number of (a) true SvSW, (b) false SvSW, (c) true NSW, and (d) false NSW events identified by IpsDst for a threshold of -250 nT in the Kyoto Dst.

(b) false SvSW, (c) true NSW, and (d) false NSW identified by IpsDst for a threshold of -250 nT in the Kyoto Dst. Following Kohavi & Provost (1998), we calculate an accuracy $[(a+c)/(a+b+c+d)]$ of 99.9% for the identification of SvSW and NSW events together and a true SvSW identification rate $[a/(a+b)]$ of 100% with only one false NSW. The false NSW corresponds to the event on 1972 August 4, which has a small IpsDst and is actually as SvSW event (Figure 5). We discuss this event in greater detail below.

4.1. SvSW Event on 1972 August 4

As reported by Anderson et al. (1974) and Albertson & Thorson (1974), a communication cable system outage and electric power supply problems occurred in the US during the rapid changes in the magnetic field during the large geomagnetic storm on 1972 August 4. Although no solar wind and IMF data were available, measurement of the time delay between the solar flare onset and shock arrival at 1 au gives the fastest ever recorded speed of ~ 2850 km s^{-1} for the ICME

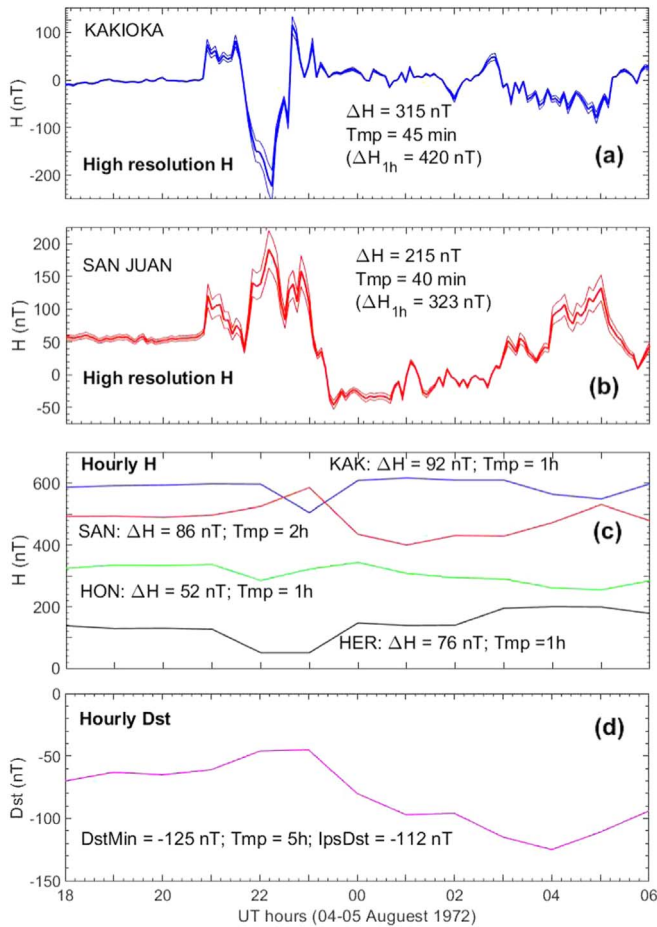


Figure 9. Scaled values (5 minute resolution) of the H-component magnetograms on 1972 August 4–5 at the Dst stations (a) Kakioka and (b) San Juan with standard deviations; zero corresponds to baseline levels of 30,094 nT and 27,440 nT, respectively. The corresponding (c) hourly H values at all four Dst stations used for computing the (d) Dst index are shown. Important parameter values are listed.

shock (Vaisberg & Zastenker 1976), which might have compressed the magnetopause to $\sim 5R_E$ (Anderson et al. 1974; Lanzerotti 1992). Study of the Pioneer 10 data at ~ 2 au showed that the average IMF B_z was around zero with considerable north–south fluctuations, and the geomagnetic storm was probably caused by a southward B_z fluctuation following the fast ICME shock (Tsurutani et al. 1992). The calculations by Tsurutani et al. (1992), assuming a solar wind speed of 2000 km s^{-1} and magnetopause compression to $5R_E$, show a high storm-time ring current peak intensity corresponding to -295 nT . K_p reached its highest values of 9; AE data are not available. Model calculations by Boteler & Beek (1999) showed that the outages were due to a rapid intensification of the electrojet current, as is typical for other SvSW events. The high impulsive action of the fastest ICME shock followed by the short-duration B_z southward seems to account for this SvSW event. If B_z had been southward for a longer period covering the ICME shock or ICME front, this event could have caused devastating effects.

The Dst storm (Figure 9(d)) has MPO at 23 UT (Dst -45 nT in the Kyoto Dst) and DstMin (-125 nT) at 04 UT, giving a T_{MP} of 5 hr and IpsDst of -112 nT , which is low compared to the IpsDst of other SvSW events. The hourly values of the corresponding H components (Figure 9(c)) used for

calculating the Dst also have low H ranges ($\Delta H = 52\text{--}92 \text{ nT}$), although their durations (1–2 hr) are shorter than T_{MP} (5 hr). To better understand the IpsDst value, the H-component magnetograms at the Dst stations Kakioka and San Juan, available at <http://wdc.kugi.kyoto-u.ac.jp/film/index.html>, are manually scaled four times at 5 minute intervals. The scaled values are digitized using the baseline values of 30,094 nT and 27,440 nT, respectively, and scale conversion factors provided by the observatories (M. Nose 2018, private communication). The four H values at each time step are used to obtain their mean and standard deviation (up to $\sim 15\%$). The time variations of H (Figures 9(a) and (b)) show large ΔH over very short durations (315 nT in 45 minutes at Kakioka and 215 nT in 40 minutes at San Juan), translating into ΔH_K of 420 nT and ΔH_S of 325 nT in 1 hr. The ΔH values are used to calculate the Dst (Sugiura & Kamei 1991) as $Dst = (1/2)(\Delta H_K / \cos(26.0) + \Delta H_S / \cos(29.9))$, with 26.0 and 29.9 being the dip latitudes at Kakioka and San Juan. It gives a 1 hr Dst (and IpsDst) of $\sim -421 \text{ nT}$. This is an approximate value because we could not use the magnetograms at Honolulu and Hermanus, which have poor quality, and could not apply the Sq correction, which requires H values for the previous five years.

To check the effect of high-resolution data further, we use the SymH index, which has been available since 1981 at <http://wdc.kugi.kyoto-u.ac.jp/aeasy>, to calculate IpsSymH. It is similar to IpsDst, but calculated for the SymH index of 1 minute resolution derived using the H-component data from 12 low-latitude stations (Iyemori et al. 1992). The distribution of IpsSymH (not shown) is similar to that of IpsDst (Figure 5); and it appears that IpsSymH may be superior to IpsDst in its ability to distinguish between SvSW and SNW. Further studies using high-resolution Dst (at least since 1958) are required to calculate the likelihood that a given IpsDst will actually cause SvSW or NSW, which is planned as described below.

4.2. SvSW Events Prior to the Dst Era

In addition to the SvSW events in 1958–2007 and the Carrington event investigated in Section 3, the SvSW events reported occurring prior to the Dst era also seem to agree with the criterion of large IpsDst. Love (2018) reported widespread problems that occurred in telegraph and telephone systems in the US on 1882 November 17. The simultaneous magnetograms recorded at the nearby station Los Angeles ($40^\circ 88'N$ magnetic) showed a 1 hr average ΔH of 470 nT, T_{MP} of 5 hr, and large dH/dt . Using Bombay magnetograms, they (Love 2018) estimated a DstMin of -386 nT . The aa index, which is a simple three-hourly global geomagnetic activity index available since 1868 and derived from two approximately antipodal observatories in Australia and the UK (Mayaud 1972), averaged to its highest value of 215 nT. These characteristics indicate a large IpsDst ($< -250 \text{ nT}$). Ribeiro et al. (2016) described widespread problems occurring in the telegraph communication networks in two mid-latitude countries (Portugal and Spain) on 1903 October 31. The magnetic field recorded simultaneously in these countries showed a large storm (similar to the Quebec storm of 1989 March 13) with H ranges over 500 nT and large dH/dt , indicating that the corresponding IpsDst could have been $< -250 \text{ nT}$. As reviewed by Cliver & Dietrich (2013), the event on 1921 May 14–15 caused telephone cable burning in Sweden and a fire at the Central New England Railroad Station switchboard in the US. Based on simultaneous magnetograms,

Kappenman (2006) estimated a DstMin ~ -850 nT for this storm, which indicates a large IpsDst. The magnetic storms on 1940 March 24 and 1941 September 19, which caused electric power supply and telecommunication problems in the US (Davidson 1940 and Love & Coïsson 2016) and when Kp reached 9, are also estimated to have large IpsDst and DstMin (< -250 nT; unpublished Dst data, J. J. 2018, private communication).

We plan to digitize the analog magnetograms available since 1904 at the four Dst stations at high time resolution (e.g., 5 minutes), compute the Dst data, automatically identify the Dst storms, and obtain the IpsDst and other important storm parameters. The magnetograms available at Cape Town will be used for the period prior to 1940 when the same are not available for the closest Dst station Hermanus. We will study how well the high-resolution storm parameters work in identifying the reported SvSW events, including minor technological problems since 1904. We expect that the high-resolution IpsDst will enable us to calculate the likelihood that a given IpsDst will actually cause SvSW or NSW. In short, the high-resolution IpsDst could be a very useful parameter for investigating different aspects of space weather.

4.3. Physical Mechanism

The mechanism of large IpsDst (high-energy input over a short duration) probably takes place through continuous and rapid magnetic reconnection (e.g., Borovsky et al. 2008). This important physical process seems to happen when there is a simultaneous occurrence of high solar wind velocity V ($\gtrsim 700$ km s $^{-1}$) coupled with a high ICME front velocity ΔV (sudden increase by over 275 km s $^{-1}$) and sufficiently large IMF Bz southward during the velocity increase ΔV (Balan et al. 2014). The importance of the coincident velocity increase and IMF Bz southward is illustrated in Figure 10. It displays the IpsDst of the 13 super storms (in the Kyoto Dst) since 1998, the Carrington super storm, and the 1972 August 4 storm (number 15) and corresponding ICME and IMF drivers in increasing order of IpsDst. The $\langle V_{MP} \rangle$ of the Carrington and 1972 August 4 SvSW events is limited to 1600 km s $^{-1}$ and their ΔV is limited to 1200 km s $^{-1}$. The solar wind velocity and IMF Bz data for the Carrington, Quebec, 1958 February, and 1972 August events (numbers 1–3 and 15) are adopted from the theoretical calculations by Cliver & Svalgaard (2004), Nagatsuma et al. (2015), Cliver et al. (1990), and Vaisberg & Zastenker (1976), respectively. An IMF Bz of -10 nT is assumed for the 1972 August 4 event following Tsurutani et al. (1992).

The red histograms correspond to SvSW and blue histograms to NSW. As shown, IpsDst has (nearly) the same distribution as the product $\langle V_{MP} \rangle \times \langle B_{ZMP} \rangle$ (Figures 10(a) and (b)), except for event number 15 (1972 August 4) because of its high $\langle V_{MP} \rangle$. The SvSW events 1–5 and 15 have both high $\langle V_{MP} \rangle$ (Figure 10(c)) and large $\langle B_{ZMP} \rangle$ southward (Figure 10(d)), as well as high ΔV (Figure 10(e)) and $B_{Z\Delta V}$ southward during the time of large ΔV (Figure 10(f)). Their combined action leads to large IpsDst. $\langle B_{ZMP} \rangle$ southward opens the dayside magnetopause and high ΔV (and high $\langle V_{MP} \rangle$) provides the force for the impulsive entry of a large number of high-energy charged particles into the magnetosphere and ring current. For NSW events (blue), the product $\langle V_{MP} \rangle \times \langle B_{ZMP} \rangle$ is comparatively small. Their striking difference compared to SvSW events is small ΔV (except for events 9 and 14) and Bz generally northward at the time of ΔV , so that either their impulsive action is weak or the strong action becomes ineffective. The

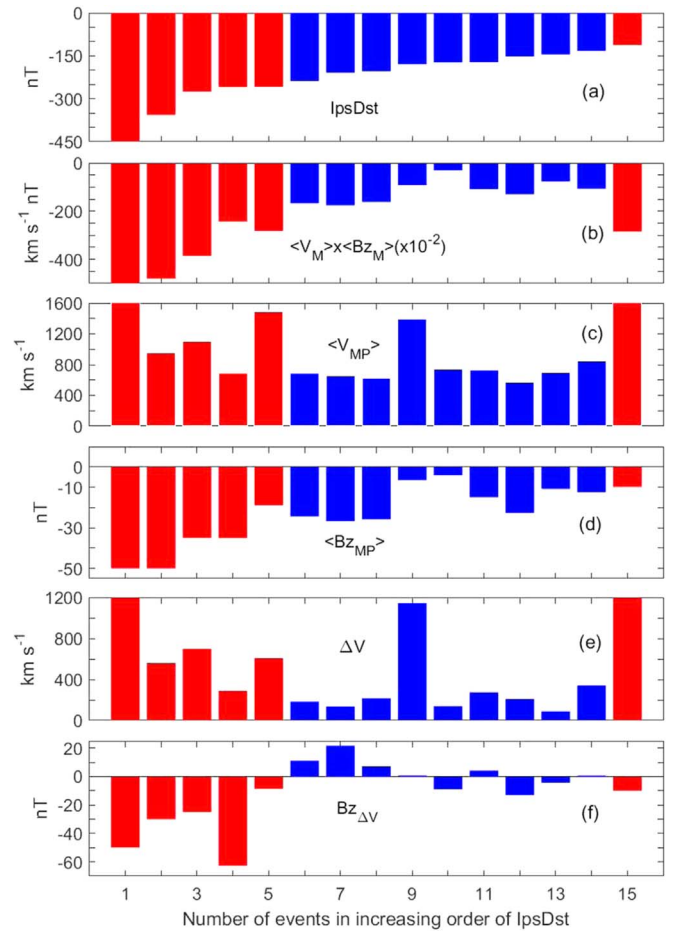


Figure 10. IpsDst of the super Dst storms (Kyoto Dst) since 1998, Carrington storm (number 1), and 1972 August storm (number 15) and corresponding $\langle V_{MP} \rangle \times \langle B_{ZMP} \rangle$, $\langle V_{MP} \rangle$, $\langle B_{ZMP} \rangle$, ΔV , and $B_{Z\Delta V}$ obtained from ACE data and adopted from theoretical values available in the literature (see text). All parameters are arranged in increasing order of IpsDst, with red for SvSW.

coincidence of high $\langle V_{MP} \rangle$ with high ΔV and simultaneous large $\langle B_{ZMP} \rangle$ southward leading to a steep decrease of Dst and large IpsDst was modeled (Balan et al. 2017a) using the comprehensive ring current model of Fok et al. (2001). The model also showed that a high $\langle V_{MP} \rangle$ not associated with a large ΔV and large $\langle B_{ZMP} \rangle$ southward does not lead to large IpsDst. In Figure 10, the 1972 August 4 SvSW event is identified by $\langle V_{MP} \rangle \times \langle B_{ZMP} \rangle$ but not by IpsDst because IMF Bz remained southward only for a short duration of less than one hour, as discussed in Section 4.1. It is also worth noting that while IpsDst is useful for identifying SvSW in ground data, the solar parameter $V \times B_z$ showing a sharp negative spike exceeding a threshold is useful for forecasting SvSW with a maximum warning time of ~ 35 minutes using ACE satellite data (Balan et al. 2017a).

The coherence of the global parameters (high ΔV and large Bz southward) leading to another global parameter (large IpsDst) and a regional phenomenon (SvSW) reveals an impulsive solar wind-magnetosphere-ionosphere coupling, which seems essential for SvSW (Figure 10). The impulsive coupling results in an intense regional ionospheric current somewhere at high latitudes (e.g., Boteler & Beek 1999), which generates strong magnetic fields reaching down to Earth, which in turn induce strong currents and voltages in Earth systems (e.g., Viljanen et al. 2010). These induced currents and voltages that exceed the tolerance limits of

the systems cause system failures (e.g., Albertson et al. 1974; Lanzerotti 1983). Finally, it should be mentioned that the global parameter IpsDst can only identify SvSW and cannot indicate the time and location of the system damages, which also depend on the regional ionospheric and ground conductivities and characteristics of the systems (power grids and telecommunication networks).

5. Summary

1. The parameter IpsDst = $(-1/T_{MP}) \int_{T_{MP}} |D_{stMP}| dt$ gives the mean value of the Dst during the storm MP. Its value decreases with increasing energy input ($\int_{T_{MP}} |D_{stMP}| dt$) and decreasing duration of energy input (T_{MP}), and therefore indicates the impulsive strength of Dst storms, while DstMin and $(dD_{st}/dt)_{MPmax}$ represent only their intensity at a single point in time.
2. IpsDst captures many important processes (ICME shock, magnetopause compression, SSC, and energy input) related to the physical mechanism (high-energy input over a short duration) that cause the sudden intensification of high-latitude ionospheric currents, leading to SvSW and resulting in electric power outages and telecommunication system failures.
3. IpsDst is derived for the Dst storms that are automatically identified in the Kyoto Dst and USGS Dst data for a period of 50 yr (1958–2007). The IpsDst in both indices seems to distinguish four of the five SvSW events (and the Carrington event) in more than 750 NSW events that occurred in 1958–2007, although the indices have significant offset of up to -70 nT in the Dst and differences of up to -54 nT in the DstMin and -58 nT in the IpsDst. The storm parameters DstMin, $(dD_{st}/dt)_{MPmax}$, AE_{max} , Kp_{max} , $\langle AE_{MP} \rangle$, and $\langle Kp_{MP} \rangle$ can identify only one or two of the SvSW events. Using an IpsDst threshold of -250 nT in the Kyoto Dst, we demonstrate a 100% true SvSW identification rate with only one false NSW.
4. The single SvSW event that occurred during a non-super storm on 1972 August 4 that appears low impulsive in Dst data (has a low value of IpsDst) is identified as a false NSW. It is also highly impulsive, as revealed by the large H ranges (420 and 325 nT) of short durations (1 hr) that are observed in the available magnetograms at two Dst stations. The results indicate that it may be useful to consider high-resolution IpsDst in the future.
5. The mechanism of large IpsDst is investigated using the solar wind velocity V and IMF Bz measured by the ACE satellite since 1998. The mechanism involves the coincidence of high $\langle V_{MP} \rangle$ containing a high ICME front velocity ΔV (sudden increase by over 275 km s $^{-1}$) and large $\langle B_{ZMP} \rangle$ southward covering ΔV . Their combined impulsive action can cause impulsive entry of a large amount of high-energy charged particles into the magnetosphere and ring current through continuous and rapid magnetic reconnection, leading to large IpsDst and SvSW through impulsive solar wind-magnetosphere-ionosphere-ground system coupling.

We thank the referee of this paper for the critical comments and helpful suggestions that have improved the quality of the paper. They deserve to be a co-author. We also thank M. Nose and T. Iyemori of Kyoto University (WDC) for the scientific

discussions and magnetograms on 1972 August 4–5 recorded at the Dst observatories at Kakioka, San Juan, Honolulu, and Hermanus, which are available at <http://www.kakioka-jma.go.jp/en/index.html>, <https://geomag.usgs.gov/> and <http://www.sansa.org.za/spacescience>, respectively. We acknowledge the use of the Kyoto Dst and USGS Dst data available at <http://wdc.kugi.kyoto-u.ac.jp/dstdir/> and <http://geomag.usgs.gov/data>, and the SymH index available at <http://wdc.kugi.kyoto-u.ac.jp/aeasy>. This research was supported by the National Key R&D Program of China (2018YFC1407304, 2018YFC1407303), the National Natural Science Foundation of China (grants 41604139, 41574138, 41774166, 41431072, 41831072), the Chinese Meridian Project, the foundation of National Key Laboratory of Electromagnetic Environment (grants 6142403180102, 6142403180103) and JSPS KAKENHI (15H05815 and 16H06286) in Japan. Work at Los Alamos was performed under the auspices of the U.S. Department of Energy with support from the NASA-ACE program.

ORCID iDs

N. Balan  <https://orcid.org/0000-0001-7079-887X>
R. Skoug  <https://orcid.org/0000-0003-1991-2643>

References

- Albertson, V. D., & Thorson, J. M. 1974, *ITPAS*, **93**, 1025
 Albertson, V. D., Thorson, J. M., & Miske, S. A. 1974, *ITPAS*, **93**, 1031
 Anderson, C. W., Lanzerotti, L. J., & MacLennan, C. G. 1974, *BSTJ*, **53**, 1817
 Aran, A., Sanahuja, B., & Lario, D. 2005, *AnGp*, **23**, 3047
 Baker, D. N., Balstad, R., Bodeau, J. M., et al. 2008, *Severe Space Weather Events: Understanding Societal and Economic Impacts* (Washington, DC: The National Academies Press), **1**
 Balan, N., Batista, I. S., TulasiRam, S., & Rajesh, P. K. 2016, *GSL*, **3**, 3
 Balan, N., Ebihara, Y., Skoug, R., et al. 2017a, *JGRA*, **122**, 2824
 Balan, N., Skoug, R., TulasiRam, S., et al. 2014, *JGRA*, **119**, 10041
 Balan, N., TulasiRam, S., Kamide, Y., et al. 2017b, *EP&S*, **69**, 59
 Borovsky, J. E., Hesse, M., Birn, J., & Kuzentsova, M. M. 2008, *JGRA*, **113**, A07210
 Boteler, D. H. 2001, in *Space Weather*, ed. P. Song, H. Singer, & G. L. Siscoe (Washington, DC: American Geophysical Union), **347**
 Boteler, D. H., & Beek, G. J. 1999, *GeoRL*, **26**, 577
 Burlage, L., Sittler, E., Mariani, F., & Schwenn, R. 1981, *JGR*, **86**, 6673
 Burton, R. K., McPherron, R. L., & Russell, C. T. 1975, *JGR*, **80**, 4204
 Carrington, R. C. 1859, *MNRAS*, **20**, 13
 Cid, C., Palacios, J., Saiz, E., Guerrero, A., & Cerrato, Y. 2014, *JSWSC*, **4**, A28
 Cliver, E. W., & Dietrich, W. F. 2013, *JSWSC*, **3**, A31
 Cliver, E. W., Feynman, J., & Garrett, H. B. 1990, *JGR*, **95**, 17103
 Cliver, E. W., & Svalgaard, L. 2004, *SoPh*, **224**, 407
 Davidson, W. F. 1940, *Edison Electr. Inst. Bull.*, **365**
 Eastwood, J. P., Biffis, E., Hapgood, M. A., et al. 2017, *Risk Anal.*, **37**, 206
 Ebihara, Y., Fok, M.-C., Sazykin, S., et al. 2005, *JGRA*, **110**, A09S22
 Fok, M.-C., Wolf, R. A., Spiro, R. W., & Moore, T. E. 2001, *JGR*, **106**, 8417
 Gonzalez, W. D., Joselyn, J. A., Kamide, Y., et al. 1994, *JGR*, **99**, 5771
 Gopalswamy, N., Yashiro, S., Michalek, G., et al. 2005, *GeoRL*, **32**, L12S09
 Green, J. C., Likar, J., & Shprits, Y. 2017, *SpWea*, **15**, 804
 Hapgood, M. A. 2011, *AdSpR*, **47**, 2059
 Iyemori, T., Araki, T., Kamei, T., & Takeda, M. 1992, *Midlatitude Geomagnetic Indices ASY and SYM (provisional) No. 1 1989*, Kyoto University
 Kamide, K., & Balan, N. 2016, *GSL*, **3**, 10
 Kappenman, J. G. 2003, *SpWea*, **1**, 1016
 Kappenman, J. G. 2006, *AdSpR*, **38**, 188
 Klimas, A. J., Vassiliadis, D., & Baker, D. N. 1997, *JGR*, **102**, 26993
 Kohavi, R., & Provost, F. 1998, *Mach. Learn.*, **30**, 127
 Lanzerotti, L. 1992, *GeoRL*, **19**, 1991
 Lanzerotti, L. J. 1983, *SSRv*, **34**, 347
 Liemohn, M. W., Jazowski, M., Kozyra, J. U., et al. 2010, *RSPSA*, **466**, 3305
 Loomis, E. 1861, *AmJS*, **94**, 71
 Love, J. J. 2018, *SpWea*, **16**, 37

- Love, J. J., & Coisson, P. 2016, *Eos*, 97, 18
- Love, J. J., & Gannon, J. L. 2009, *AnGeo*, 28, 3101
- Love, J. J., Lucas, G. M., Kelbert, A., & Bedrosian, P. A. 2017, *GeoRL*, 45, 5
- Love, J. J., Rigler, E. J., Pulkkinen, A., & Riley, P. 2015, *GeoRL*, 42, 6544
- Lühr, H., Xiong, C., Olsen, N., & Le, G. 2017, *SSRv*, 206, 521
- Marshall, R. A., Dalzell, M., Waters, C. L., Goldthorpe, P., & Smith, E. A. 2012, *SpWea*, 10, S08003
- Mayaud, P. N. 1972, *JGR*, 77, 6870
- McComas, D. J., Bame, S. J., Barker, P., et al. 1998, *SSRv*, 86, 563
- Medford, L. V., Lanzerotti, L. J., Kraus, J. S., & MacLennan, C. G. 1989, *GeoRL*, 16, 1145
- Nagatsuma, T., Kataoka, R., & Kunitake, M. 2015, *EP&S*, 67, 78
- Newell, P. T., Sotirelis, T., Liou, K., Meng, C.-I., & Rich, F. J. 2007, *JGRA*, 112, A01206
- Pulkkinen, A., Lindahl, S., Viljanen, A., & Pirjola, R. 2005, *SpWea*, 3, S08C03
- Pulkkinen, T. 2007, *LRSP*, 4, 1
- Ribeiro, P., Vaquero, J. M., Gallego, M. C., & Trigo, R. M. 2016, *SpWea*, 14, 464
- Rostoker, G., Samson, J. C., Creutzberg, F., et al. 1995, *SSRv*, 46, 743
- Schrijver, C. J., Kauristie, K., Aylward, A. D., et al. 2015, *AdSpR*, 55, 2745
- Singh, A. K., Singh, D., & Singh, R. P. 2010, *SGeo*, 31, 581
- Skoug, R. M., Gosling, J. T., Steinberg, J. T., et al. 2004, *JGRA*, 109, A09102
- Slothower, J. C., & Albertson, V. D. 1967, *J Minn. Acad. Sci.*, 34, 94
- Smith, E. J., & Wolfe, J. H. 1976, *GeoRL*, 3, 137
- Sugiura, M. 1964, *Ann. Int. Geophys. Year*, 35, 9
- Sugiura, M., & Kamei, T. 1991, *Equatorial Dst Index 1957–1986*, IAGA Bulletin 40, International Service of Geomagnetic Indices
- Svalgaard, L. 1977, in *Coronal Holes and High Speed Wind Streams*, ed. J. B. Zirker (Boulder, CO: Colorado Association Univ. Press), 371
- Tsurutani, B. T., Gonzalez, W. D., Tang, F., et al. 1992, *GeoRL*, 19, 1993
- Tsurutani, B. T., Gonzalez, W. D., Lakhina, G. S., & Alex, S. 2003, *JGRA*, 108, 1268
- Vaisberg, O. L., & Zastenker, G. N. 1976, *SSRv*, 19, 687
- Viljanen, A., Koistinen, A., Pajunpää, K., et al. 2010, *Geoph*, 46, 59
- Wik, M., Pirjola, R., Lundstedt, H., et al. 2009, *AnGeo*, 27, 1775
- Witasse, O., Sanchez-Cano, B., Mays, M. L., et al. 2017, *JGRA*, 122, 7865
- Zhu, D., Billings, S. A., Balikhin, M. A., Wing, S., & Alleyne, H. 2007, *JGRA*, 112, A06205